Combined Experimental and Theoretical Approach To Understand the Reactivity of a Mononuclear Cu(II)−Hydroperoxo Complex in Oxygenation Reactions†

Takashi Kamachi,‡ Yong-Min Lee,§ Tomonori Nishimi,‡ Jaeheung Cho,§ Kazunari Yoshizawa,*,‡ and Wonwoo Nam*,§

Institute for Materials Chemistry and Engineering, Kyushu University, Fukuoka 812-8581, Japan, and Department of Chemistry and Nano Science, Ewha Womans University, Seoul 120-750, Korea

Received: May 30, 2008; Revised Manuscript Received: September 8, 2008

A copper(II) complex bearing a pentadentate ligand, $[Cu^{II}(N4Py)(CF_3SO_3)_2]$ (**1**) (N4Py = *N*,*N*-bis(2-pyridylmethyl)bis(2-pyridyl)methylamine), was synthesized and characterized with various spectroscopic techniques and X-ray crystallography. A mononuclear Cu^{II}−hydroperoxo complex, $[Cu^{II}(N4Py)(OOH)]^+$ (**2**), was then generated in the reaction of **1** and H_2O_2 in the presence of base, and the reactivity of the intermediate was investigated in the oxidation of various substrates at −40 °C. In the reactivity studies, **2** showed a low oxidizing power such that **2** reacted only with triethylphosphine but not with other substrates such as thioanisole, benzyl alcohol, 1,4-cyclohexadiene, cyclohexene, and cyclohexane. In theoretical work, we have conducted density functional theory (DFT) calculations on the epoxidation of ethylene by **2** and a $[Cu^{III}(N4Py)(O)]^+$ intermediate (**3**) at the B3LYP level. The activation barrier is calculated to be 39.7 and 26.3 kcal/mol for distal and proximal oxygen attacks by **2**, respectively. This result indicates that the direct ethylene epoxidation by **2** is not a plausible pathway, as we have observed in the experimental work. In contrast, the ethylene epoxidation by **3** is a downhill and low-barrier process. We also found that **2** cannot be a precursor to **3**, since the homolytic cleavage of the O−O bond of **2** is very endothermic (i.e., 42 kcal/mol). On the basis of the experimental and theoretical results, we conclude that a mononuclear Cu^{II}−hydroperoxo species bearing a pentadentate N5 ligand is a sluggish oxidant in oxygenation reactions.

1. Introduction

The mechanism of catalytic oxygenation of hydrocarbons mediated by copper monooxygenases, such as peptidylglycine α-hydroxylating monooxygenase (PHM) and dopamine β-monooxygenase (Dβ M), attracts much attention in the communities of bioinorganic and biological chemistry.[1−3] These enzymes catalyze the activation of substrate C−H bonds (e.g., a glycine backbone C−H bond in PHM or a dopamine benzylic C−H bond in Dβ M) by using molecular oxygen in a stereo- and regiospecific manner.[4−7] Although it has been well established that mononuclear copper centers at the active sites play important roles in O_2-binding, activation, and the hydroxylation of substrates,[8] their catalytic mechanism still remains elusive.

In earlier studies,[6,9] a Cu^{II}−hydroperoxo species, which is generated by the protonation of a Cu^{I}−superoxo species, was proposed to cleave the C−H bond of substrate via a concerted process. The cleavage of the O−O bond of the Cu^{II}−hydroperoxo species prior to substrate activation was suggested to be unlikely due to the high redox potential for the $1e^-$ oxidation of Cu(II) → Cu(III).[6] Tian et al. proposed the involvement of an oxo-mediated radical mechanism that was derived from the study of oxygen-18 kinetic isotope effects.[10] In their mechanism the Cu^{II}−hydroperoxo species abstracts a hydrogen atom from a nearby tyrosine residue to produce a Cu−oxo (Cu(II)−O$^{\bullet}$ ↔ Cu(III)=O^{2-}) species, a tyrosyl radical, and a water molecule. The produced Cu-oxo species then participates in oxidation reactions.

Recently, Cu^{II}−superoxo species have been proposed as reactive intermediates in the activation of substrate C−H bonds.[1c,3b,11] This mechanism involves an initial hydrogen atom (H-atom) abstraction from substrate by the Cu^{II}−superoxo species, thereby generating Cu^{II}−hydroperoxo and substrate-free radical as intermediates. Chen and Solomon conducted density functional theory (DFT) calculations to understand the nature of reactive intermediates in the dioxygen activation and substrate C−H bond hydroxylation by PHM.[12] Two possible intermediates, such as Cu^{II}−hydroperoxo and Cu^{II}−superoxo species, were evaluated in the activation of substrate C−H bonds. The Cu^{II}−hydroperoxo species was found to be a less plausible intermediate for the substrate C−H activation, with a high activation energy of 37 kcal/mol for the H-atom abstraction from formylglycine, a substrate model. In contrast, the substrate H-atom abstraction by the Cu^{II}−superoxo species was thermodynamically favorable with an activation barrier of 14 kcal/mol, thus leading to the conclusion that the Cu^{II}−superoxo species is the reactive species in the PHM reaction.

More recently, Kamachi et al. studied dopamine hydroxylation by the Cu^{II}−superoxo, Cu^{II}−hydroperoxo, and Cu^{III}−oxo species of Dβ M to understand the nature of the active species in the hydroxylation of dopamine.[13] They constructed a 3D model of Dβ M for QM/MM calculations using homology modeling techniques and revealed the functions of key amino acid residues in the active site of the enzyme. Yoshizawa et al. also carried out QM/MM calculations to obtain better information on the reactivity of the Cu^{II}−superoxo and Cu^{III}−oxo species in the

† Part of the "Sason S. Shaik Festschrift".

* Authors to whom correspondence should be addressed. E-mail: wwnam@ewha.ac.kr (W.N.) and kazunari@ms.ifoc.kyushu-u.ac.jp (K.Y.).
‡ Kyushu University.
§ Ewha Womans University.

10.1021/jp804804j CCC: $40.75
Published on Web 11/08/2008

protein environment.[14] Their calculations suggested that the Cu^{III}−oxo species, which is generated by the O−O bond homolysis of the Cu^{II}−hydroperoxo species, is the most reactive species in the activation of the benzylic C−H bond of dopamine. Crespo et al.[15] recently proposed that a Cu−oxo species, $[L^{\bullet+}Cu(II)O^{\bullet-}]^{2+}$, which is generated by the heterolytic O−O bond cleavage of Cu^{II}−hydroperoxo species, would be the actual active species in the H-atom abstraction by PHM.

There have been significant advances recently in biomimetic studies of mononuclear copper-active oxygen complexes.[3] Karlin and co-workers provided the first spectroscopic evidence that a copper(I) complex binds dioxygen to form an end-on Cu^{II}−superoxo species,[16] as seen in X-ray structures of PHM and a model complex.[17] The Cu^{II}−superoxo species undergoes oxygenation reactions with phenols at −85 °C and shows the ^{18}O-incorporation from an $^{18}O_2$-labeled Cu^{II}−superoxo complex into products. The reactivity of mononuclear Cu^{II}−hydroperoxo complexes bearing tetradentate ligands has also been investigated in the oxidative N-dealkylation and aryl hydroxylation reactions.[18,19] Although the intermediates disappeared upon the addition of substrates, it is not clear at this moment whether the Cu^{II}−hydroperoxo complexes or derived species (e.g., Cu^{III}−oxo species) are the true oxidants. Very recently, Tolman and co-workers prepared Cu^{I}−α-ketocarboxylate complexes that react with O_2 to generate active copper−oxygen intermediates.[20] These intermediates show reactivity in the hydroxylation of an arene substituent on the supporting N-donor ligand.[20] On the basis of theoretical calculations, Cu^{II}−peracid and Cu^{III}−oxo species were proposed as active oxidants in this reaction. More recently, Itoh and co-workers investigated the reactivity of a Cu^{II}−cumylperoxo complex in the oxidation of 10-methyl-9,10-dihydroacridine ($AcrH_2$) and 1,4-cyclohexadiene (CHD).[21] They observed a large kinetic isotope effect of $k_H/k_D = 19.2$ in the hydride transfer reaction of $AcrH_2$ and the formation of benzene in the C−H activation of CHD. They proposed the involvement of a mononuclear copper(II)−oxyl radical species, $LCu^{II}-O^{\bullet}$, which is generated by the O−O bond homolysis of the Cu^{II}−cumylperoxo complex, in the oxidation of organic substrates.

In this work, we synthesized a copper(II) complex bearing a pentadentate N5 ligand, $Cu^{II}(N4Py)(CF_3SO_3)_2$ (**1**) (N4Py = *N*,*N*-bis(2-pyridylmethyl)bis(2-pyridyl)methylamine), and the corresponding Cu^{II}−hydroperoxo complex, $[Cu^{II}(N4Py)(OOH)]^+$ (**2**). The reactivity of the Cu^{II}−hydroperoxo complex was investigated in various oxidation reactions. We also conducted DFT calculations on olefin epoxidation by the intermediate. On the basis of the experimental and theoretical results, we propose that the Cu^{II}−hydroperoxo species bearing a pentadentate ligand is a sluggish oxidant in oxygenation reactions.

2. Experimental and Theoretical Methods

Chemicals and Physical Measurement. All chemicals obtained from Aldrich Chemical Co. were the best available purity and used without further purification unless otherwise indicated. Solvents were dried according to published procedures and distilled under Ar prior to use.[22] H_2O_2 (30 wt % solution in water) and $Cu(CF_3SO_3)_2$ were obtained from Aldrich Chemical Co., and the N4Py ligand was prepared by literature methods.[23]

All reactions were followed by monitoring UV−vis spectral changes of reaction solutions with a Hewlett-Packard 8453 spectrophotometer equipped with an Optostat^{DN} variable-temperature liquid-nitrogen cryostat (Oxford instruments). Electrospray ionization mass spectra (ESI-MS) were collected on a Thermo Finnigan (San Jose, CA, USA) LCQ Advantage MAX quadrupole ion trap instrument, by infusing samples directly into the source using a manual method. The spray voltage was set at 4.2 kV and the capillary temperature at 120 °C. EPR spectra were acquired at X-band frequency and at 4 K by using a JEOL JES-FA200 spectrometer. The scan rate and time constant were chosen such that the product of scan rate (gauss/s) and time constant(s) was much less than the smallest line width in the spectrum. The field modulation frequency was 100 kHz.

X-ray Crystallographic Determination. X-ray crystallographic analysis was carried out with a Bruker SMART APEX CCD diffractometer. The diffraction data for **1** were collected at 273(2) K on a Bruker SMART AXS diffractometer equipped with a monochromator in the Mo Kα ($\lambda = 0.71073$ Å) incident beam.[24a] The CCD data were integrated and scaled by using the Bruker-SAINT software package, and the structure was solved and refined with SHELX-97.[24b] The full-matrix least-squares program used minimized $\sum w(F_o - F_c)^2$; the weight (w) of an observation was the reciprocal square of $\sigma(F_c)$, its standard deviation. All esds (except the esd in the dihedral angle between two ls planes) are estimated by using the full covariance matrix. H atoms were geometrically positioned and fixed. The absorption corrections were not applied for the *hkl* data because the crystal shape was uniform. Some displacement ellipsoids elongated along the bonds might be attributable to the nonabsorption corrections. Crystallographic data for the structures reported here have been deposited with the Cambridge Crystallographic Data Centre (Deposition No. CCDC-688772).

Generation and Reactivity of a Cu(II)−Hydroperoxo Complex. The mononuclear copper(II) complex $[Cu^{II}(N4Py)(CH_3CN)(CF_3SO_3)_2]$ (**1**) was synthesized by reacting equimolar amounts of $Cu(CF_3SO_3)_2$ and N4Py ligand in CH_3CN at room temperature. Blue crystals of **1** suitable for crystallographic analysis were obtained from CH_3CN/diethyl ether. The mononuclear Cu(II)−hydroperoxo intermediate, $[Cu^{II}(N4Py)(OOH)]^+$ (**2**), was prepared by reacting **1** with 5 equiv of H_2O_2 in the presence of 2.5 equiv of triethylamine in CH_3CN at −40 °C. The formation of **2** was characterized with a UV−vis spectrophotometer and EPR. **2** was then used in reactivity studies with appropriate amounts of substrates at −40 °C. All reactions were followed by monitoring UV−vis spectral changes of reaction solutions, and reaction rates were determined under pseudo-first-order reaction conditions.

DFT Calculations. We carried out density functional theory (DFT) calculations to evaluate the reactivities of Cu^{II}−hydroperoxo and Cu^{III}−oxo species using the Jaguar program package.[25] Calculations were performed by using the B3LYP hybrid density functional method[26] in combination with the LACVP basis set[27] for Cu and the 6-31G* basis set[28] for the rest of the atoms. Solvent effect calculations were done with the polarized continuum model (PCM) as implemented in the Jaguar program with a dielectric constant $\varepsilon = 35.7$ for acetonitrile.

3. Results and Discussion

Generation and Reactivity of a Cu(II)−Hydroperoxo Intermediate. The mononuclear copper(II) complex, $[Cu^{II}(N4Py)(CF_3SO_3)_2]$ (**1**), was synthesized by reacting equimolar amounts of $Cu(CF_3SO_3)_2$ and N4Py ligand in CH_3CN, and its blue single crystals suitable for crystallographic analysis were obtained by the diffusion of diethyl ether into the reaction solution. The X-ray structure of **1** shows a six-coordinate copper(II) center with a distorted octahedral geometry, and the copper(II) center was deviated by 0.35 Å toward the atom N6 from the equatorial

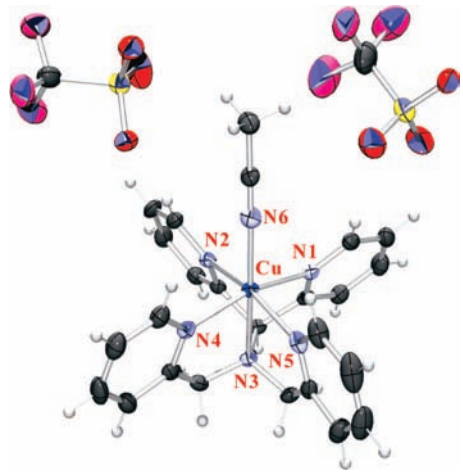

Figure 1. ORTEP diagram of $[Cu^{II}(N4Py)(CF_3SO_3)_2]$ (**1**) showing the selected atom-numbering scheme and 30% probability ellipsoids. Selected bond distances (Å): Cu−N1 2.087(3), Cu−N2 2.108(3), Cu−N3 2.206(3), Cu−N4 2.055(3), Cu−N5 2.072(3), Cu−N6 2.130(3).

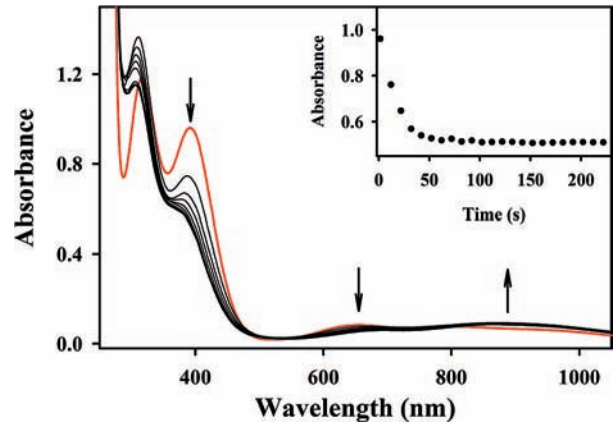

Figure 2. UV−vis spectrum of $[Cu^{II}(N4Py)(OOH)]^+$ (**2**) (0.5 mM) (red line), and the spectral changes upon the addition of PEt_3 (15 mM) in CH_3CN at −40 °C. The inset shows absorbance traces monitored at 392 nm.

plane [N1−N2−N4−N5] (Figure 1). The dihedral angle between the N1−Cu−N4 plane and the N2−Cu−N5 plane is 89.10(10)°. The crystal structure of **1** is quite similar to that of the iron analogue reported previously,[23,29] but the average Cu−N distance in **1** is significantly longer than the average Fe−N distance in the iron analogue. Especially, the $Cu-N_{CH_3CN}$ and $Cu-N_{amine}$ distances are much longer than the $Fe-N_{CH_3CN}$ and $Fe-N_{amine}$ distances by 0.205 and 0.227 Å, respectively, as a result of the severe Jahn−Teller effect operating on the d^9 configuration of copper(II). The ESI-MS of **1** exhibits a prominent ion peak at a mass-to-charge ratio (*m*/*z*) of 579.1, whose mass and isotope distribution pattern corresponds to $[Cu^{II}(N4Py)(CF_3SO_3)]^+$ (calculated *m*/*z* of 579.1) (Supporting Information (SI), Figure S1a). The X-band EPR spectrum of **1** has been recorded at 4 K (Figure S1b, SI) and exhibits intense signals at $g_{||} = 2.220$ with $A_{||} = 178.1 \times 10^{-4}$ cm^{-1} and $g_{\perp} = 2.072$, indicating that the geometry around the cooper(II) atom is five-coordinate and distorted square pyramidal in the solution phase due to the displacement of the CH_3CN ligand.

Complex **1** was then reacted with H_2O_2 to generate the corresponding Cu^{II}−hydroperoxo complex, $[Cu(II)(N4Py)(OOH)]^+$ (**2**), by following the previously reported method for the generation of Cu^{II}−OOH species.[18,19,30] Upon addition of 5 equiv of H_2O_2 to a reaction solution containing **1** and triethylamine (Et_3N) in CH_3CN at −40 °C, the color of the solution changed from blue to green. The UV−vis spectrum of the intermediate **2** exhibits an intense absorption band at 392 nm ($\varepsilon = 1950$ M^{-1} cm^{-1}) due to the peroxo-to-copper(II) charge transfer transition (LMCT) together with the weak d−d bands at 665 and 823 nm (Figure 2).[18,19,30] These λ_{max} values together with the ε values indicate the generation of a Cu^{II}−OOH species; UV−vis spectra of Cu^{II}−OOH species exhibit an intense band in the range of 360−420 nm with an ε value in the range of 800−2000 M^{-1} cm^{-1} and weak d−d bands at 660−820 nm in CH_3CN.[18,19,30] The X-band EPR spectrum of **2** at 4 K exhibits intense signals at $g_{||} = 2.190$ with $A_{||} = 80.8 \times 10^{-4}$ cm^{-1} and $g_{\perp} = 2.094$ with $A_{\perp} = 64.2 \times 10^{-4}$ cm^{-1}, indicating that the geometry around the cooper(II) atom is a six-coordinate and distorted octahedral structure (Figure S2, SI).

The intermediate **2** decayed slowly at −40 °C ($k_{obs} = 7.3 \times 10^{-4}$ s^{-1}) (Figure S3a, SI), and the plot of the natural decay of **2** against 1/*T* allowed us to determine the activation parameters of ΔH and $\Delta S^{\ddagger}$ to be 43 kJ mol^{-1} and −119 J K^{-1} mol^{-1}, respectively (Figure S3b, SI). Then, the reactivity of the intermediate **2** at −40 °C was investigated with various substrates, including triethylphosphine (PEt_3) for *P*-oxidation, thioanisole for *S*-oxidation, benzyl alcohol for alcohol oxidation, 1,4-cyclohexadiene and cyclohexane for C−H activation, and cyclohexene for olefin epoxidation. The intermediate reacted with PEt_3 (Figure 2), which is known as one of the easiest substrates in oxygenation reactions, but not with other substrates (Table S2, SI). By carrying out reactions with different PEt_3 concentrations, second-order rate constants were determined to be $k_2 = 4.6$ M^{-1} s^{-1} at −40 °C for **2** (Figure S4, SI). In this section, we have reported experimental results, such as the synthesis of a copper(II) complex bearing a pentadentate N4Py ligand and the generation and characterization of its Cu^{II}−hydroperoxo intermediate. We have also demonstrated that the Cu^{II}−hydroperoxo species with a pentadentate N5 ligand is a sluggish oxidant in oxygenation reactions.

Reactivity of a Cu(II)−Hydroperoxo Species. Figure 3 shows a computed potential-energy profile for ethylene epoxidation by $[Cu^{II}(N4Py)(OOH)]^+$ (**2**). There are two possible entrance channels for this reaction, a distal oxygen attack and a proximal oxygen attack by **2**. In the initial stages of the reaction pathways, **2** forms a reactant complex ($\mathbf{RC_{OOH}}$) with an ethylene molecule, followed by a transition state for the distal oxygen attack ($\mathbf{TS1_{distal}}$) or by a transition state for the proximal oxygen attack ($\mathbf{TS1_{proximal}}$). The O−O bond of the hydroperoxo ligand is cleaved, and the distal oxygen atom is transferred to one of the carbon atoms of ethylene in $\mathbf{TS1_{distal}}$. The activation energy for $\mathbf{TS1_{distal}}$ is 39.7 kcal/mol when measured from $\mathbf{RC_{OOH}}$. The energy of radical intermediate ($\mathbf{I1_{distal}}$) is >20 kcal/mol higher than that of $\mathbf{RC_{OOH}}$. On the other hand, an ethylene molecule approaches the proximal oxygen atom and a covalent bond is formed between the oxygen atom and a carbon atom of ethylene in $\mathbf{TS1_{proximal}}$, leading to a radical intermediate ($\mathbf{I1_{proximal}}$). Isomerization of $\mathbf{I1_{proximal}}$ to $\mathbf{I2_{proximal}}$ may occur through exchange of the Cu−O bonds to weaken the O−O bond. The resultant intermediate easily goes to the product complex ($\mathbf{PC_{proximal}}$) via $\mathbf{TS2_{proximal}}$. The activation energy for the proximal oxygen attack is estimated to be 26.3 kcal/mol relative to $\mathbf{RC_{OOH}}$, which is significantly lower than that in $\mathbf{TS1_{distal}}$. However, these values are rather high for olefin epoxidation reactions, e.g. 9.3 kcal/mol for compound I of cytochrome P450[31] and 9.9 kcal/mol for an Fe−oxo complex $[Fe^{IV}{=}O(TPA)(CH_3CN)]^{2+}$.[32] These calculational results indicate that

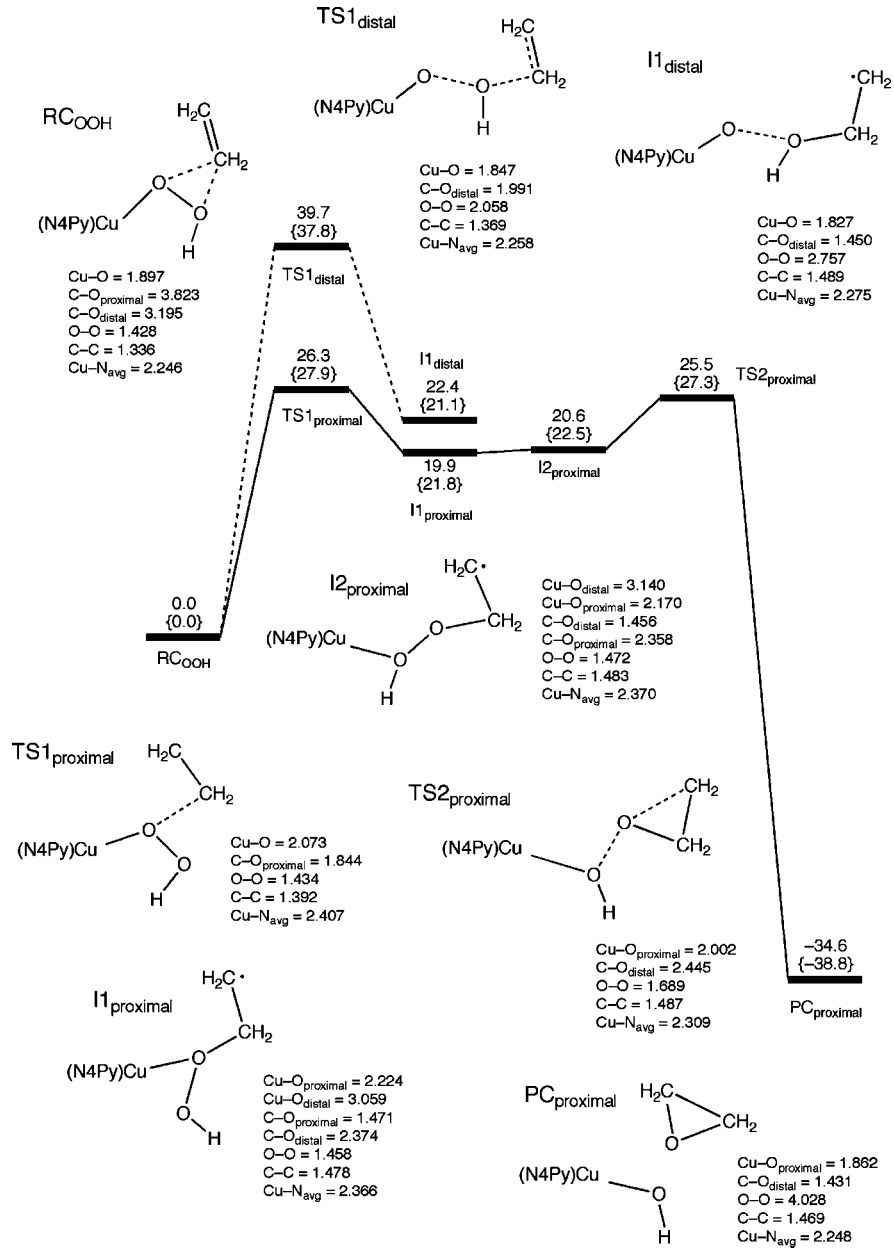

Figure 3. Energy diagram for ethylene epoxidation by the Cu^{II}−hydroperoxo complex in the doublet state. Energies in curly brackets include solvation correction (using a dielectric constant of $\varepsilon = 35.7$ for acetonitrile). Energies in kcal/mol and bond lengths in Å.

2 cannot participate in this reaction directly, due to the high energy barriers for the distal and proximal oxygen attacks.

Olefin Epoxidation by a Cu(III)−Oxo Species. As discussed in the previous section, the Cu^{II}−hydroperoxo species does not have sufficient oxidizing power for ethylene epoxidation. We here look at the possibility of the ethylene epoxidation by a Cu^{III}−oxo species that is generated via the O−O bond homolysis of the Cu^{II}−hydroperoxo species (vide supra). Figure 4 shows a computed potential-energy profile for ethylene epoxidation by the Cu^{III}−oxo complex, $[Cu^{III}(N4Py)(O)]^+$ (**3**). There are two closely lying spin states in the Cu−oxo species ($\mathbf{RC_{oxo}}$), triplet and singlet states, which correspond respectively to the ferromagnetic and antiferromagnetic coupling of unpaired electrons on the Cu atom and the oxo ligand. B3LYP calculations predicted that the triplet state is 4.4 kcal/mol lower than the singlet state. The spin densities of the Cu atom and the oxo ligand were calculated to be 0.6 (−0.6) and 1.3 (0.7) in the triplet (singlet) state, respectively. The formation of a covalent bond between the oxo ligand and a carbon atom of ethylene via $\mathbf{TS1_{oxo}}$ yields a radical intermediate $\mathbf{I_{oxo}}$, which has an unpaired electron on the terminal CH_2 group. The activation barriers for the C−O bond formation were calculated to be only 3.1 and 3.3 kcal/mol in the triplet and singlet states, respectively. This barrier is rather low compared with a corresponding barrier of 9.9 kcal/mol for an Fe−oxo complex $[Fe^{IV}{=}O(TPA)(CH_3CN)]^{2+}$.[32] Thus, **3** easily oxidizes ethylene via the transition state $\mathbf{TS1_{oxo}}$ with an exothermal energy of nearly 20 kcal/mol. This transition state has a Cu−O bond of 1.861 (1.853) Å and a C−O bond of 2.052 (2.131) Å in the triplet (singlet) state. The triplet and singlet spin states of the resultant radical intermediate $\mathbf{I_{oxo}}$ are close in energy because the unpaired electron on the carbon radical center, which determines its spin state, has almost no magnetic interaction with the Cu atom.

The second half of the epoxidation reaction is the ring-closure process, in which a covalent bond is formed between the oxygen atom and the other carbon atom of ethylene to form the product complex $\mathbf{PC_{oxo}}$. The activation energy was calculated to be 31.7 kcal/mol on the triplet surface, while this process is barrierless

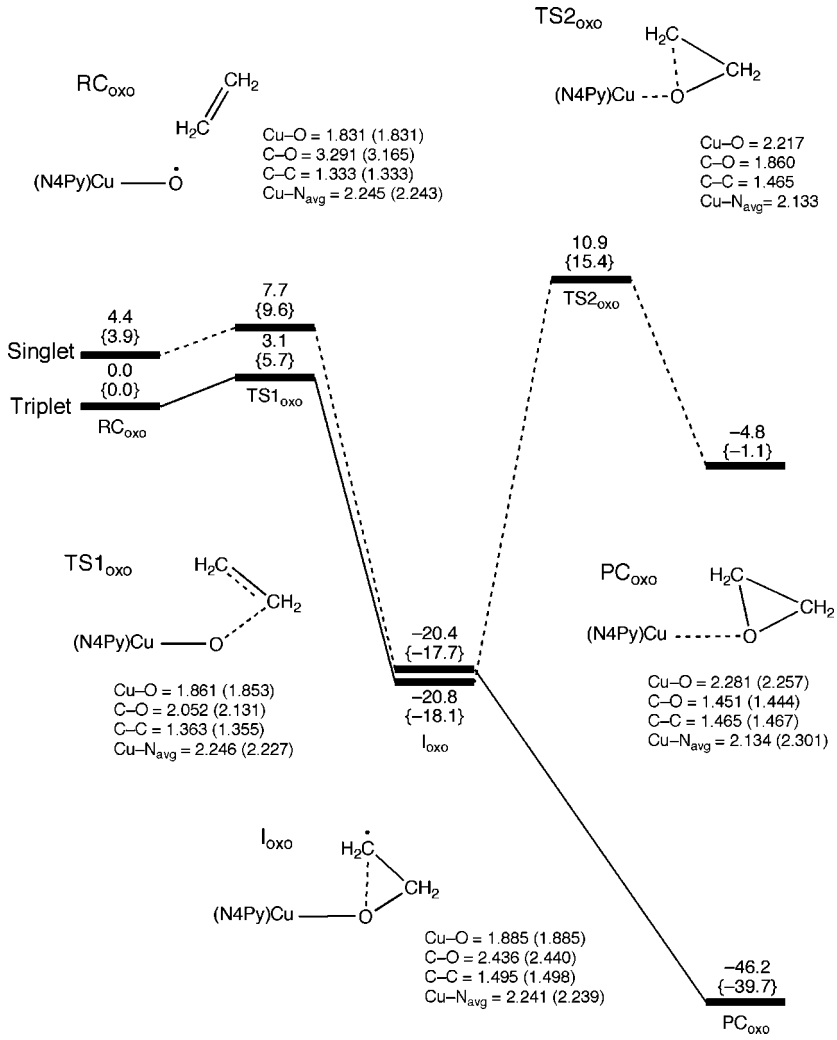

Figure 4. Energy diagram for ethylene epoxidation by the Cu^{III}−oxo complex in the singlet and triplet states. Energies in curly brackets include solvation correction (using a dielectric constant of $\varepsilon = 35.7$ for acetonitrile). Energies in kcal/mol and bond lengths in Å.

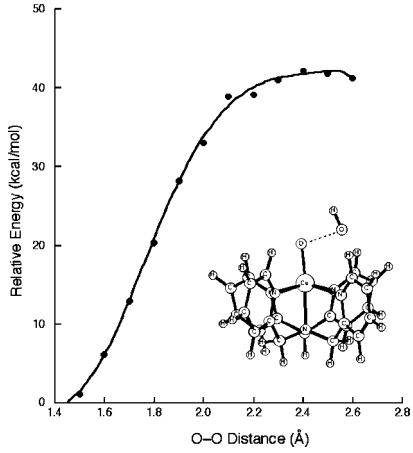

Figure 5. Energy profile for the O−O bond cleavage of the Cu^{II}−hydroperoxo complex.

on the singlet potential energy surface, which is in good agreement with previous theoretical results that alkane hydroxylation by a Cu−oxo species of DβM occurs effectively in a concerted manner on the singlet surface.[13,14] We scanned the quintet potential energy surface from $\mathbf{I_{oxo}}$ to the product complex $\mathbf{PC_{oxo}}$ to confirm that this ring closure proceeds in a barrierless fashion, as collected in Supporting Information (Figure S5). The high barrier on the triplet potential energy surface comes from the reduction of Cu(II) to Cu(I). The ground state of the Cu(I) atom has a closed-shell d^{10} configuration, and the triplet d^9s^1 excited state is 66 kcal/mol higher than the singlet d^{10} state.[33] Thus, the transition state and final product complex involve the unstable electronic configuration of the Cu atom in the triplet state. These calculational results suggest that a spin inversion from the triplet state to the single state would take place when the radical intermediate $\mathbf{I_{oxo}}$ goes down the slope of the barrierless potential energy surface. The overall reaction by **3** is highly exothermic, and the transition states involved are low-lying; therefore, this reaction is readily mediated by **3**.

O−O Bond Homolysis of the Cu(II)−Hydroperoxo Species. 3 has a strong oxidation capability toward olefin as discussed above. However, the participation of **3** in olefin epoxidation has not been proved experimentally yet, and the mechanism of its formation is not clear at the present time and the detection of mononuclear Cu^{III}−oxo species is a big challenge in bioinorganic copper chemistry.[34] In this section, we will give an answer why it is so difficult to capture the Cu−oxo species. The O−O bond of the Cu−hydroperoxo complex is homolytically cleaved in aprotic solvent. To explore the energy profile of the O−O bond homolysis, we scanned the potential energy surface along the O−O coordinate using partial optimization. As shown in Figure 5, a high activation energy of 42 kcal/mol is required to overcome the steep energy barrier. This value is 16 and 2 kcal/mol higher than those for

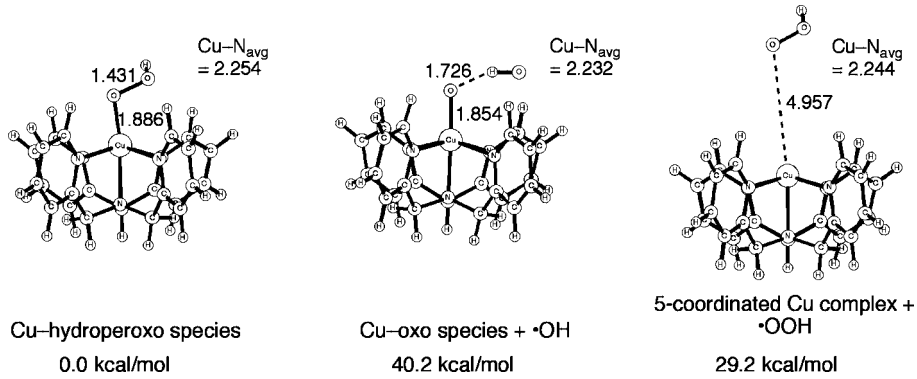

Figure 6. Optimized structures of the Cu^{II}−hydroperoxo species and intermediates generated by the O−O and Cu−O bond cleavage.

the proximal and distal oxygen attacks, respectively. Figure 6 shows fully optimized structures of the Cu^{II}−hydroperoxo species and the Cu^{III}−oxo species that is weakly bonded to the •OH radical. The Cu−oxo species is unstable by 40.2 kcal/mol, compared to the Cu−hydroperoxo species. We also computed the energy profile of the O−O bond homolysis adding a water molecule to see if the presence of water traces affects the stability of the Cu−hydroperoxo species. As summarized in the SI, Figure S6, the water molecule has no impact on the stabilization of intermediates and the transition state. Internal electron transfers occur to reduce the Cu−oxygen species in the catalysis of PHM and DβM. To evaluate the effect of the electron donation to the reaction system we computed the bond dissociation energy of the O−O bond of the Cu(I)−hydroperoxo complex to form the Cu(I)−O• complex. The bond dissociation energy is calculated to be 50.7 kcal/mol at the B3LYP level of theory. These results clearly demonstrate that it is more difficult to cleave the O−O bond of the Cu−hydroperoxo complex in contrast to that of the Fe−alkylperoxo complex.[32] Actually, the deactivation of reactive copper intermediates would preferentially occur via the Cu−O bond cleavage, resulting in the release of •OOH radical, as shown in Figure 6. These results imply that clever catalytic strategies must be devised to weaken the O−O bond of the Cu−hydroperoxo species. Hong et al.[20] designed the Cu−α-ketocarboxylate complexes that are converted into the Cu−peracid complexes with loss of CO_2. The Cu−peracid complex with a weak O−O bond would have a better chance to generate the reactive Cu−oxo complex via the homolytic cleavage of the O−O bond.[31] In summary, our DFT calculations demonstrate that the Cu^{II}−hydroperoxo species with a pentadentate N5 ligand is a sluggish oxidant that does not effect the olefin epoxidation and that the generation of a highly reactive Cu^{III}−oxo species via the O−O bond activation is thermodynamically unfavorable.

4. Conclusions

In this study, we have examined the reactivity of a mononuclear Cu^{II}−hydroperoxo species bearing a pentadentate N5 ligand from experimental and theoretical approaches. A mononuclear Cu^{II}−hydroperoxo complex was prepared and investigated in the oxygenation of various substrates. The Cu^{II}−hydroperoxo complex exhibits a reactivity with triethylphosphine, which is one of the easiest substrates in oxygenation reactions. In theoretical work, we have investigated the olefin epoxidation by the Cu^{II}−hydroperoxo and Cu^{III}−oxo species using B3LYP calculations. The energy barrier for the olefin epoxidation by the Cu^{II}−hydroperoxo species is high, indicating that this intermediate is not capable of oxygenating olefins. In contrast, the Cu−oxo complex easily mediates the olefin epoxidation with a low energy barrier. However, the homolytic cleavage of the O−O bond of the Cu−hydroperoxo complex is very endothermic, indicating that the formation of the Cu−oxo species is not thermodynamically favorable. The present experimental and theoretical results demonstrate that the Cu^{II}−hydroperoxo complex with a pentadentate N5 ligand is not responsible for the oxygenation of organic substrates.

Acknowledgment. T.K. acknowledges a Grant-in-Aid for Young Scientists (No. 18750048) from the Japan Society for the Promotion of Science (JSPS). K.Y. thanks Grants-in-Aid for Scientific Research (Nos. 18350088, 18066013, and 18GS0207) from the Japan Society for the Promotion of Science, the Kyushu University Global-COE project of the Ministry of Culture, Sports, Science, and Technology of Japan (MEXT) and the Nanotechnology Support Project of MEXT, the Joint Project of Chemical Synthesis Core Research Institutions of MEXT, and CREST of the Japan Science and Technology Cooperation. W.N. is grateful for financial support from KOSEF/MOST through Creative Research Initiative Program. The authors thank Professor Edward I. Solomon and Ms. Julia Woertink at Stanford University for their attempt to obtain resonance Raman spectra of the copper(II)−hydroperoxo complex.

Supporting Information Available: Crystallographic, kinetic, and spectroscopic data for the copper complexes, calculated energy profile for ring closure, and optimized structures of all the reaction species. This material is available free of charge via the Internet at http://pubs.acs.org.

References and Notes

(1) (a) Ljones, T.; Skotland, T. In *Copper Proteins and Copper Enzymes*; Lontie, R., Ed.; CRC Press: Boca Raton, FL, 1984; Vol. *2*, pp 131−157. (b) Klinman, J. P. *Chem. Rev.* **1996**, *96*, 2541. (c) Klinman, J. P. *J. Biol. Chem.* **2006**, *281*, 3013.

(2) Eipper, B. A.; Stoffers, D. A.; Mains, R. E. *Annu. Rev. Neurosci.* **1992**, *15*, 57.

(3) (a) Lewis, E. A.; Tolman, W. B. *Chem. Rev.* **2004**, *104*, 1047. (b) Decker, A.; Solomon, E. I. *Curr. Opin. Chem. Biol.* **2005**, *9*, 152. (c) Balasubramanian, R.; Rosenzweig, A. C. *Acc. Chem. Res.* **2007**, *40*, 573. (d) Itoh, S.; Fukuzumi, S. *Acc. Chem. Res.* **2007**, *40*, 592. (e) Suzuki, M. *Acc. Chem. Res.* **2007**, *40*, 609.

(4) Fitzpatrick, P. F.; Villafranca, J. J. *J. Am. Chem. Soc.* **1985**, *107*, 5022.

(5) Miller, S. M.; Klinman, J. P. *Biochemistry* **1983**, *22*, 3091.

(6) Miller, S. M.; Klinman, J. P. *Biochemistry* **1985**, *24*, 2114.

(7) Wimalasena, K.; May, S. W. *J. Am. Chem. Soc.* **1989**, *111*, 2729.

(8) Stewart, L. C.; Klinman, J. P. *Annu. Rev. Biochem.* **1988**, *57*, 551.

(9) Brenner, M. C.; Klinman, J. P. *Biochemistry* **1989**, *28*, 4664.

(10) Tian, G.; Berry, J. A.; Klinman, J. P. *Biochemistry* **1994**, *33*, 226.

(11) Evans, J. P.; Ahn, K.; Klinman, J. P. *J. Biol. Chem.* **2003**, *278*, 49691.

(12) (a) Chen, P.; Solomon, E. I. *J. Am. Chem. Soc.* **2004**, *126*, 4991. (b) Chen, P.; Solomon, E. I. *Proc. Natl. Acad. Sci. U.S.A.* **2004**, *101*, 13105.

(13) Kamachi, T.; Kihara, N.; Shiota, Y.; Yoshizawa, K. *Inorg. Chem.* **2005**, *44*, 4226.

(14) Yoshizawa, K.; Kihara, N.; Kamachi, T.; Shiota, Y. *Inorg. Chem.* **2006**, *45*, 3034.

(15) Crespo, A.; Martí, M. A.; Roitberg, A. E.; Amzel, L. M.; Estrin, D. A. *J. Am. Chem. Soc.* **2006**, *128*, 12817.

(16) Maiti, D.; Fry, H. C.; Woertink, J. S.; Vance, M, A.; Solomon, E. I.; Karlin, K. D. *J. Am. Chem. Soc.* **2007**, *129*, 264.

(17) (a) Prigge, S. T.; Eipper, B. A.; Mains, R. E.; Amzel, L. M. *Science* **2004**, *304*, 864. (b) Würtele, C.; Gaoutchenova, E.; Harms, K.; Holthausen, M. C.; Sundermeyer, J.; Schindler, S. *Angew. Chem., Int. Ed.* **2006**, *45*, 3867.

(18) Maiti, D.; Sarjeant, A. A. N.; Karlin, K. D. *J. Am. Chem. Soc.* **2007**, *129*, 6720.

(19) Maiti, D.; Lucas, H. R.; Sarjeant, A. A. N.; Karlin, K. D. *J. Am. Chem. Soc.* **2007**, *129*, 6998.

(20) Hong, S.; Huber, S. M.; Gagliardi, L.; Cramer, C. C.; Tolman, W. B. *J. Am. Chem. Soc.* **2007**, *129*, 14190.

(21) Kunishita, A.; Ishimaru, H.; Nakashima, S.; Ogura, T.; Itoh, S. *J. Am. Chem. Soc.* **2008**, *130*, 4244.

(22) *Purification of Laboratory Chemicals*; Armarego, W. L. F., Perrin, D. D., Eds.; Pergamon Press: Oxford, UK, 1997.

(23) Roelfes, G.; Lubben, M.; Leppard, S. W.; Schudde, E. P.; Hermant, R. M.; Hage, R.; Wilkinson, E. C.; Que, L., Jr.; Feringa, B. L. *J. Mol. Catal. A: Chem.* **1997**, *117*, 223.

(24) (a) Sheldrick, G. M. *SHELXTL/PC*, Version 6.12 for Windows XP; Bruker AXS Inc.: Madison, WI, 2001. (b) Sheldrick, G. M. *SHELXL97 & SHELXS97*, Program for the Refinement of Crystal Structures; University of Göttingen: Göttingen, Germany, 1997.

(25) *Jaguar 5.0*; Schrödinger, L.L.C.: Portland, OR, 1991−2003.

(26) (a) Becke, A. D. *Phys. Rev. A* **1988**, *38*, 3098. (b) Becke, A. D. *J. Chem. Phys.* **1993**, *98*, 5648.

(27) (a) Hay, J. P.; Wadt, W. R. *J. Chem. Phys.* **1985**, *82*, 299. (b) Friesner, R. A.; Murphy, R. B.; Beachy, M. D.; Ringnalda, M. N.; Pollard, W. T.; Dunietz, B. D.; Cao, Y. *J. Phys. Chem. A* **1999**, *103*, 1913.

(28) (a) Ditchfield, R.; Hehre, W. J.; Pople, J. A. *J. Chem. Phys.* **1971**, *54*, 724. (b) Hehre, W. J.; Ditchfield, R.; Pople, J. A. *J. Chem. Phys.* **1972**, *56*, 2257. (c) Hariharan, P. C.; Pople, J. A. *Theor. Chim. Acta* **1973**, *28*, 213.

(29) Rohde, J.-U.; Torelli, S.; Shan, X.; Lim, M. H.; Klinker, E. J.; Kaizer, J.; Chen, K.; Nam, W.; Que, L., Jr. *J. Am. Chem. Soc.* **2004**, *126*, 16750.

(30) (a) Yamaguchi, S.; Masuda, H. *Sci. Technol. Adv. Mater.* **2005**, *6*, 34. (b) Wada, A.; Harata, M.; Hasegawa, K.; Jitsukawa, K.; Masuda, H.; Mukai, M.; Kitagawa, T.; Einaga, H. *Angew. Chem., Int. Ed.* **1998**, *37*, 798. (c) Osako, T.; Nagatomo, S.; Tachi, Y.; Kitagawa, T.; Itoh, S. *Angew. Chem., Int. Ed.* **2002**, *41*, 4325. (d) Fujii, T.; Naito, A.; Yamaguchi, S.; Wada, A.; Funahashi, Y.; Jitsukawa, K.; Nagatomo, S.; Kitagawa, T.; Masuda, H. *Chem. Commun.* **2003**, 2700. (e) Fujii, T.; Yamaguchi, S.; Funahashi, Y.; Ozawa, T.; Tosha, T.; Kitagawa, T.; Masuda, H. *Chem. Commun.* **2006**, 4428.

(31) Kamachi, T.; Shiota, Y.; Ohta, T.; Yoshizawa, K. *Bull. Chem. Soc. Jpn.* **2003**, *76*, 721.

(32) (a) Seo, M. S.; Kamachi, T.; Kouno, T.; Murata, K.; Park, M. J.; Yoshizawa, K.; Nam, W. *Angew. Chem., Int. Ed.* **2007**, *46*, 2291. (b) Park, M. J.; Lee, J.; Suh, Y.; Kim, J.; Nam, W. *J. Am. Chem. Soc.* **2006**, *128*, 2630.

(33) Moore, C. E. *Atomic Energy Levels*; U.S. National Bureau of Standards:Washington, DC, 1949; circular 467.

(34) Itoh, S. *Curr. Opin. Chem. Biol.* **2006**, *10*, 115.

JP804804J